Microscopic effective reaction theory for deuteron-induced reactions

Yuen Sim Neoh,[*] Kazuki Yoshida, Kosho Minomo, and Kazuyuki Ogata

Research Center for Nuclear Physics, Osaka University, Ibaraki 567-0047, Japan

The microscopic effective reaction theory is applied to deuteron-induced reactions. A reaction model space characterized by a $p + n + A$ three-body model is adopted, where A is the target nucleus, and the nucleon-target potential is described by a microscopic folding model based on an effective nucleon-nucleon interaction in nuclear medium and a one-body nuclear density of A. The three-body scattering wave function in the model space is obtained with the continuum-discretized coupled-channels (CDCC) method, and the eikonal reaction theory (ERT), an extension of CDCC, is applied to the calculation of neutron removal cross sections. Elastic scattering cross sections of deuteron on ^{58}Ni and ^{208}Pb target nuclei at several energies are compared with experimental data. The total reaction cross sections and the neutron removal cross sections at 56 MeV on 14 target nuclei are calculated and compared with experimental values.

I. INTRODUCTION

Projectile-breakup reactions have been utilized for studying the structures of nuclei, in the field of physics of unstable nuclei in particular. One of the most successful models for describing breakup processes of a nucleus into a few fragments is the continuum-discretized coupled-channels (CDCC) method [1–3]. The theoretical foundation of CDCC through its relation to the distorted-wave Faddeev theory was given in Refs. [4,5]. Recently, progress has been made to construct scattering potentials employed in the CDCC calculation from a microscopic point of view. This attempt can be interpreted as an application of the microscopic reaction theory [3], which is based on the multiple scattering theory for nucleus-nucleus scattering [6], to reaction processes involving a weakly bound projectile, by setting an appropriate model space. Very recently, a microscopic description of the projectile wave function also has been reported [7]. Such a microscopic description of breakup processes is crucial for quantitative determination of structure of unstable nuclei from reaction observables.

In this work, we discuss the breakup of a deuteron, the simplest composite nucleus, to examine the microscopic effective reaction theory, i.e., CDCC with an appropriate reaction model space and the microscopic nucleon-nucleus (N-A) optical potentials. Nowadays, N-A scattering observables can be described microscopically with no free adjustable parameter [8–10]. It is thus expected that the microscopic CDCC calculation can describe deuteron elastic scattering data that have successfully been reproduced by CDCC with phenomenological N-A optical potentials [1]. It should be pointed out that the model in the present study differs from a fully microscopic calculation such as those of the *ab initio* method [11]. The limitation of the three-body model description compared with a many-body reaction theory can be seen in, e.g., Ref. [12]. Nevertheless, the deuteron elastic scattering and its elastic breakup processes have successfully been described by CDCC, a three-body reaction model, with phenomenological optical potentials. The purpose of the present study is to implement microscopic optical potentials in the usual CDCC calculation. This can be regarded as an *effective* microscopic reaction model based on a three-body model.

It should be noted that the deuteron breakup states in the intermediate channel, i.e., the virtual breakup of the deuteron, were shown to be crucial for describing the deuteron elastic scattering [1,2]. Convergence of the CDCC results with respect to the p-n relative orbital angular momentum ℓ (including odd partial waves) is discussed as well as the Coulomb breakup contribution. Furthermore, we apply the eikonal reaction theory (ERT) [13] with microscopic optical potentials, microscopic ERT, to the calculation of the total reaction cross sections σ_R and the neutron removal cross sections σ_{-n} on various target nuclei measured at 28 MeV/nucleon [14]. ERT is an extension of CDCC for inclusive breakup observables and can be interpreted as also the extension of the Glauber model to explicitly take into account the p-A Coulomb interaction, hence the Coulomb breakup effects on those observables.

In Sec. II, we describe the method of microscopic CDCC, followed by the methodology used to extract inclusive neutron removal cross section using ERT. The numerical results of microscopic CDCC and ERT are presented in Sec. III. In Sec. IV we give a summary.

II. FRAMEWORK

As deuteron is well known to be a weakly bound nucleus consisting of proton (p) and neutron (p), deuteron-induced nuclear reactions are, as a result of an appropriate choice of the reaction model space, often treated as a $p + n + A$ three-body system. The total wave function Ψ satisfies the Schrödinger equation

$$(H - E)\Psi(\boldsymbol{R},\boldsymbol{r}) = 0, \tag{1}$$

where the coordinates $\boldsymbol{R}$ and $\boldsymbol{r}$ are defined as shown in Fig. 1 and the total Hamiltonian H is the sum of the relative kinetic operators and the potentials in the center-of-mass frame. In the
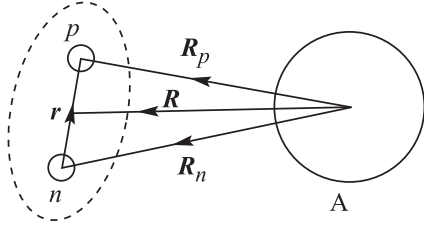
_____

*neohys@rcnp.osaka-u.ac.jp

FIG. 1. Schematics of deuteron-induced nuclear reaction system.

three-body system, the total potential is written as $V_{pn}(\boldsymbol{r}) + U_p(\boldsymbol{R}_p) + V_C(\boldsymbol{R}_p) + U_n(\boldsymbol{R}_n)$; V_{pn} is the interaction between p and n, U_p (U_n) is the nuclear potential between p (n) and A, and V_C is the Coulomb potential between p and A. A general overview of the microscopic construction of potentials U_p and U_n is given in Ref. [3]. According to that, in the present work, we adopt the microscopic nucleon-target potentials obtained by folding the Melbourne g-matrix interaction [8] with a target density in the same manner as in Ref. [15]. Target densities used in the folding procedure are obtained by the Hartree-Fock calculation with the Gogny D1S force as explained in Ref. [16]. The validity of the microscopic optical potentials for proton elastic scattering is shown in Refs. [15] and [16]. Then Eq. (1) with the microscopic optical potentials is solved by CDCC [1–3].

In our microscopic optical potential the nonlocality coming from knock-on exchange process is taken into account properly with the localization method by Brieva and Rook [16] but the potential is still energy dependent. We adopt the choice of $E_d/2$ as the energy of optical potentials in the present study. This prescription is valid for elastic scattering as discussed in Refs. [17,18]. For deuteron stripping reaction (d,p), Timofeyuk and Johnson suggested that a different choice of the energy of optical potentials is needed [18], as mentioned above. It is nontrivial whether the energy dependence of optical potential is crucial or not for other reaction observables. However, we can expect that the energy dependence coming from a nonlocal effect is not essential for elastic breakup and neutron removal reactions since such reactions are determined by the asymptotic behavior of scattering wave functions.

We denote the neutron removal cross section from the deuteron as σ_{-n}. It can be written as the sum

$$\sigma_{-n} = \sigma_{\mathrm{EB}} + \sigma_{n:\mathrm{STR}}, \tag{2}$$

where σ_{EB} is the elastic breakup cross section and $\sigma_{n:\mathrm{STR}}$ is the neutron stripping cross section; in the elastic breakup A stays in the ground state, whereas in the stripping A is excited to unspecified states. σ_{EB} is calculated with CDCC and $\sigma_{n:\mathrm{STR}}$ with ERT [13,19]. The essence of ERT is that the scattering matrix is divided into the proton and neutron parts, S_p and S_n, respectively, by using the adiabatic approximation to only U_n [19]. With S_p and S_n thus separated, we can define $\sigma_{n:\mathrm{STR}}$ as

$$\sigma_{n:\mathrm{STR}} = 2\pi \int \langle 0| \, |S_p|^2 (1 - |S_n|^2)|0\rangle b\, db, \tag{3}$$

where b is the impact parameter and $|0\rangle$ is the ground state of deuteron. Equation (3) has the simple interpretation regarding

projectile deuteron; it is the joint probability of the proton being scattered off (survival probability) and the neutron being absorbed out of the model space (absorption probability) simultaneously. From Eq. (3), one sees [19] that

$$\sigma_{n:\mathrm{STR}} = \sigma_{\mathrm{R}} - \sigma_{\mathrm{EB}} - [\sigma_{\mathrm{R}}(p) - \sigma_{\mathrm{EB}}(p)], \tag{4}$$

where $\sigma_{\mathrm{R}}(p)$ and $\sigma_{\mathrm{EB}}(p)$ are the total reaction and elastic breakup cross sections, respectively, obtained by solving Eq. (1) without U_n. Thus Eq. (2) becomes

$$\sigma_{-n} = \sigma_{\mathrm{R}} - \sigma_{\mathrm{R}}(p) + \sigma_{\mathrm{EB}}(p). \tag{5}$$

Equation (5) gives the prescription formula to obtain the inclusive neutron removal cross section from deuteron, whose components can be obtained with CDCC.

III. RESULTS AND DISCUSSION

In the description of the p-n system, we adopt a one-range Gaussian interaction [20] as V_{pn}. The intrinsic spin S of the deuteron is assumed to be zero for simplicity; the effect of such nonzero intrinsic spin will be discussed later for high-energy case. The p-n breakup states with s, p, d, f, g, h, and i partial waves are included. Each of them is discretized by the momentum-bin method with an equal increment $\Delta k = 0.1$ fm^{-1} to a maximum of $k_{\max} = 1.0$ fm^{-1}. The maximum values of r and R are 100 and 250 fm, respectively.

A. Deuteron elastic scattering

Figure 2 shows the elastic differential cross sections of deuteron scattering on ^{58}Ni at 80 MeV. Figure 3 shows the elastic scattering result of 56 MeV deuteron on ^{12}C and ^{58}Ni, while Fig. 4 shows the elastic scattering of 52 MeV deuteron on ^{16}O. The microscopic calculations show good agreement
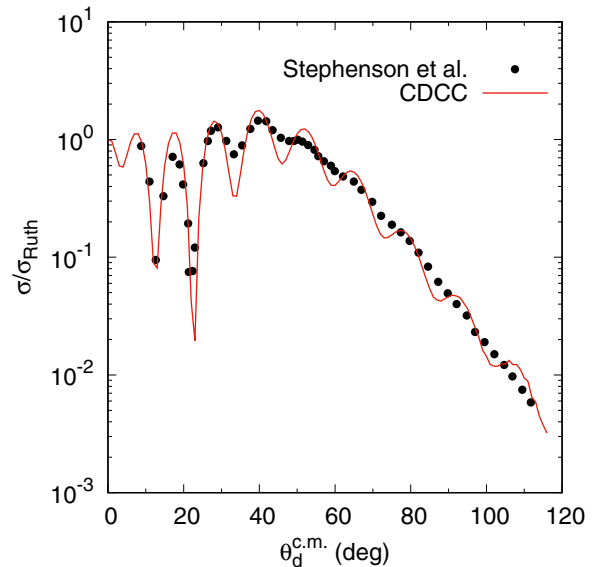

FIG. 2. Deuteron elastic scattering differential cross section normalized to the Rutherford cross section at 80 MeV on ^{58}Ni. The solid line denotes the result of the microscopic CDCC calculation. The experimental data are taken from Ref. [21].
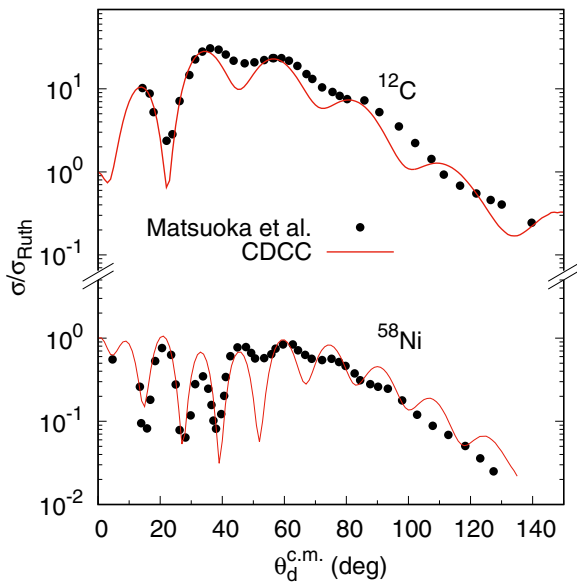
FIG. 3. Deuteron elastic scattering differential cross section normalized to the Rutherford cross section at 56 MeV on ^{12}C and ^{58}Ni. The solid lines denote the results of the microscopic CDCC calculation. The experimental data are taken from Ref. [23].

with the experimental data [21] up to the large angles without any free parameters. At these energies, the microscopic CDCC calculation shows better agreement than the previous calculation [22] with the phenomenological potential, even though the tensor coupling between the deuteron s and d states is not included here.

However, the microscopic calculation (solid line) at 21.6 MeV cannot reproduce the data at backward angles (Fig. 5). This may indicate that the microscopic optical
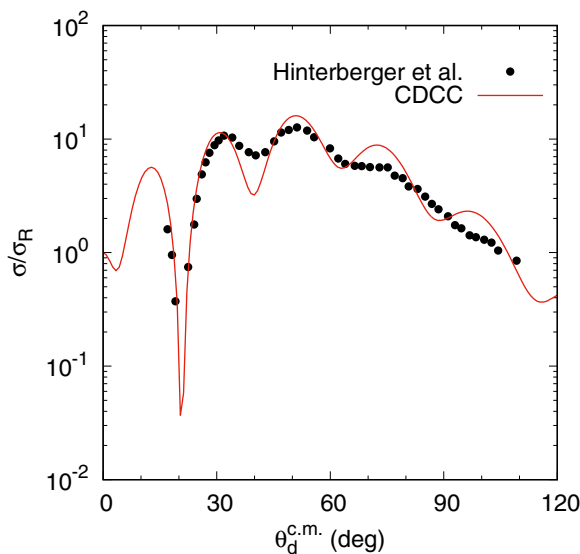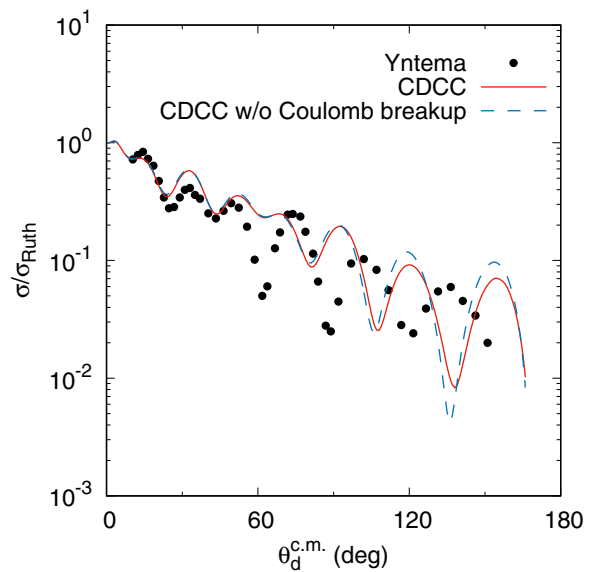

FIG. 5. Same as Fig. 2 but at 21.6 MeV. The dashed line corresponds to the result of CDCC without the Coulomb breakup. The experimental data are taken from Ref. [30].

potentials are invalid at such low energies (around 10 MeV for nucleon energy). This will be reasonable because in the folding model calculation adopted, only the knock-on exchange is taken into account. In other words, the total wave function of the nucleon-nucleus system is not fully antisymmetrized. As discussed in Ref. [25], at higher energies this treatment is justified. At low energies, however, other complicated exchange processes will become important and the present folding model procedure will lose ustification.

FIG. 4. Deuteron elastic scattering differential cross section normalized to the Rutherford cross section at 52 MeV on ^{16}O. The solid line denotes the result of the microscopic CDCC calculation. The experimental data are taken from Ref. [24].
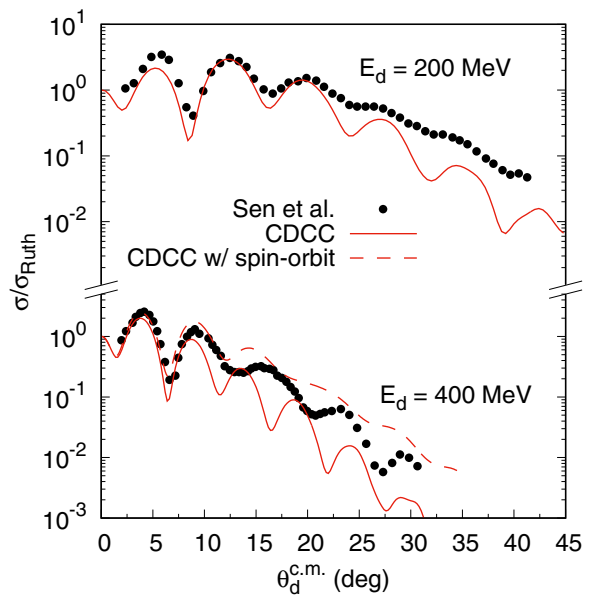

FIG. 6. Same as Fig. 2 but at 200 and 400 MeV. The dashed line is the result of microscopic CDCC with the spin-orbit interaction. The experimental data are taken from Ref. [31].
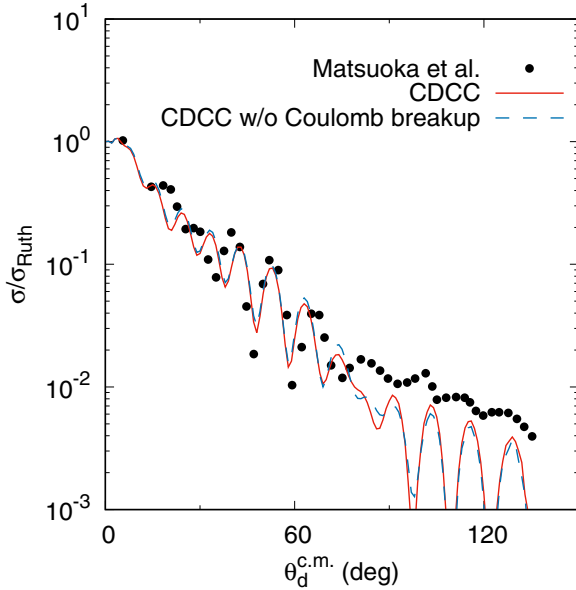
FIG. 7. Same as Fig. 5 but at 56 MeV on ^{208}Pb. The experimental data are taken from Ref. [23].

The advantage of the present calculation compared to previous studies is twofold. First, we include not only even but also odd partial ℓ waves of the p-n breakup states which are previously ignored in Refs. [22,26,27]. The odd partial waves contribute mainly to the Coulomb breakup processes that are expected to be important at lower incident energies. Second, we clarify the role of $\ell > 2$ to the elastic and breakup cross section which is not taken into account by previous studies such as those in Refs. [28,29]. In particular, we can

confirm that $\ell_{max} = 2$ is sufficiently convergent for the elastic scattering cross section but not for breakup observables, which will be discussed in more detail in Sec. III B.

We show by the dashed line in Fig. 5 the result of microscopic CDCC without Coulomb breakup. One sees that the difference is very small except at backward angles. This is also confirmed in the case on ^{208}Pb at 56 MeV, as shown in Fig. 7 below. Therefore, we can conclude that the Coulomb breakup effects are negligibly small for deuteron elastic scattering, which validates the previous studies [22,26–29]. It should be noted, however, that the Coulomb breakup effects are significant for breakup cross sections as shown in Sec. III B.

Figure 6 shows the elastic scattering cross sections of deuteron at higher energies, 200 and 400 MeV, on ^{58}Ni. The microscopic CDCC calculation (solid line) can reproduce the data fairly well at 200 MeV but it undershoots the data at 400 MeV. As mentioned above, the spin-orbit part of the microscopic optical potential has been ignored in the present study. However, it is well known that, at hundreds of MeV/nucleon, the effect of the spin-orbit potential becomes more apparent. Therefore, at 400 MeV, we perform CDCC calculation including the spin-orbit potential; we assume $S = 1$ and include the s-, p-, and d-wave breakup states. The result is shown by the dashed line in Fig. 6. One can find that the effect of the spin-orbit potential gives good agreement between the calculated and measured cross sections, at forward angles in particular. We have confirmed that the effect of the spin-orbit interaction is small in other reactions discussed in the present study.

Figure 7 shows the result at 56 MeV on ^{208}Pb. The microscopic CDCC is quite successful in reproducing the experimental data, as in Fig. 3. Even with the ^{208}Pb target, as mentioned above, the contribution of the Coulomb breakup is very small on the elastic cross section.

TABLE I. Decomposition of elastic breakup cross section into partial wave contributions from s wave to i wave. All cross sections are in units of mb.

| Target	Energy (MeV)	σ_{EB}	s	p	d	f	g	h	i
^{58}Ni	21.6	72.82	10.27	19.78	17.78	5.56	7.56	2.67	9.20
^{58}Ni	56	149.01	24.76	42.96	39.28	4.75	17.92	2.12	17.22
^{58}Ni	80	157.54	27.32	48.36	51.72	5.42	15.61	1.95	7.15
^{58}Ni	200	111.73	19.35	46.95	38.74	2.34	3.51	0.26	0.59
^{58}Ni	400	53.21	6.89	31.87	13.25	0.30	0.76	0.04	0.10
^{12}C	56	105.51	22.48	4.14	57.91	0.83	14.31	0.31	5.52
^{25}Mg	56	121.29	24.47	11.95	52.55	1.95	18.72	0.76	10.89
^{27}Al	56	115.38	22.66	13.55	48.93	2.12	17.15	0.81	10.15
^{48}Ti	56	137.84	25.21	29.56	42.67	3.45	19.06	1.54	16.35
^{51}V	56	139.88	25.31	31.29	41.65	3.65	19.41	1.61	16.96
^{54}Fe	56	146.45	24.93	38.64	40.22	4.54	18.93	1.98	17.20
^{89}Y	56	170.15	27.14	64.12	37.40	6.53	14.91	2.78	17.27
^{90}Zr	56	172.69	27.27	66.62	37.44	6.77	14.68	2.83	17.08
^{118}Sn	56	191.22	29.52	84.69	37.59	9.57	12.25	3.47	14.12
^{159}Tb	56	231.43	36.51	111.69	43.42	14.15	10.47	4.31	10.88
^{181}Ta	56	257.84	41.71	125.48	48.41	17.00	10.44	4.86	9.94
^{197}Au	56	277.90	45.78	135.73	52.63	19.15	10.35	5.22	9.04
^{208}Pb	56	287.50	49.47	139.75	55.38	18.65	10.40	5.08	8.77
^{209}Bi	56	288.93	48.01	141.80	55.05	20.36	10.10	5.41	8.20
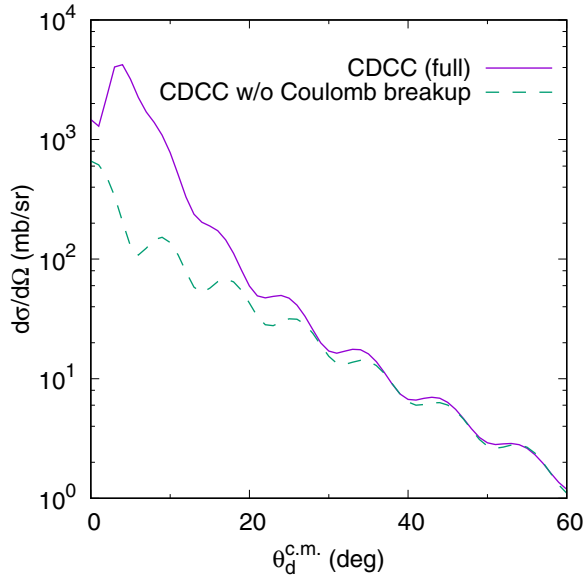
FIG. 8. Angular distribution of the total elastic breakup cross section at 56 MeV on ^{208}Pb. The solid line denotes the result of full CDCC, whereas the dashed line denotes CDCC without Coulomb breakup.

B. Breakup observables

In Table I we show the total elastic breakup cross section σ_{EB} and its decomposition into the contributions $\sigma_{EB;\ell}$ from p-n partial waves for each reaction system discussed in Sec. III A and below. As mentioned, the odd waves contribute to σ_{EB} mainly through the Coulomb breakup. Among them, the p-wave contribution $\sigma_{EB;1}$ is dominant because of the properties of the multipoles of the p-A Coulomb interaction. The contributions from $\ell = 3$ and 5 are much smaller than $\sigma_{EB;1}$, showing a clear convergence of the result with respect to odd ℓ. On the other hand, for even partial waves, the convergence is very slow at 56 MeV and lower energies. At

21.6 MeV on ^{58}Ni, $\sigma_{EB;6}$ is even larger than $\sigma_{EB;4}$. Nevertheless, fortunately, it is found that adding $\ell = 8$ gives a very small change in σ_{EB}; typically it is less than about 2% and, at maximum, it is 4.5% for the reaction at 56 MeV on ^{208}Pb. Thus we conclude that our CDCC calculation converges at $\ell_{max} = 6$ within a few percent error. To determine the role of higher partial waves $\ell > 2$ on elastic breakup cross section, we found that at 56 MeV on ^{208}Pb, σ_{EB} at $\ell_{max} = 2$ differs from that at $\ell_{max} = 6$ by about 8%, while at 21.6 MeV on ^{58}Ni their difference becomes larger by about 26%. We conclude that elastic breakup cross section does not sufficiently converge at $\ell_{max} = 2$, especially at lower energies.

At higher energies, one can directly see a clear convergence with ℓ from the values shown in Table I. Another important finding is that the Coulomb breakup plays an important role also for the light targets. In fact, the Coulomb breakup contributes as much as 18% (30%) to σ_{EB} at 56 MeV on ^{12}C (^{58}Ni). To see the role of the Coulomb breakup in more detail, we show in Fig. 8 the angular distribution of the total elastic breakup cross section at 56 MeV on ^{208}Pb. The solid line is the result of the full CDCC calculation and the dashed line is that without the p-A Coulomb interaction. As expected, the Coulomb breakup is dominant at forward angles; neglecting the Coulomb breakup decreases the breakup cross section by an order of magnitude at around 5°. Finally, we show in Table II and Fig. 9 the results of the total reaction cross sections σ_R and the neutron removal cross sections σ_{-n} of 56 MeV deuteron on 14 target nuclei. One can see that the results agree fairly well with experimental data, for σ_R in particular.

IV. SUMMARY

We have carried out CDCC calculation by employing microscopic scattering potentials, and showed that the observables obtainable from this method agree fairly well with experimental data in a wide range of energies without the need for artificial normalization or any arbitrary parameters.

TABLE II. Total reaction cross sections and neutron removal cross sections of 56 MeV deuteron on 14 target elements. Experimental data are taken from Ref. [14]. All values shown are in units of mb.

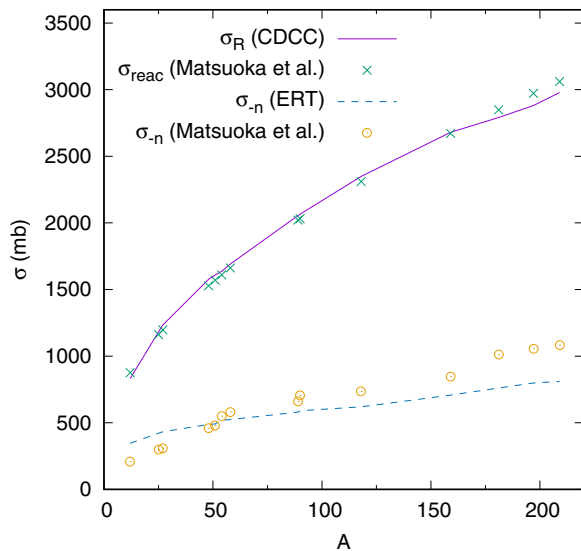| Target	Total reaction cross section, σ_R		Neutron removal cross section, σ_{-n}	
	CDCC	data	CDCC	data
^{12}C	832	876	347	209
^{25}Mg	1182	1162	422	299
^{27}Al	1234	1198	432	309
^{48}Ti	1577	1528	488	458
^{51}V	1609	1570	491	481
^{54}Fe	1637	1610	519	550
^{58}Ni	1692	1662	524	582
^{89}Y	2055	2021	580	661
^{90}Zr	2065	2032	590	705
^{118}Sn	2349	2310	620	735
^{159}Tb	2680	2671	708	847
^{181}Ta	2791	2848	761	1011
^{197}Au	2881	2972	799	1055
^{209}Bi	2978	3061	810	1082

FIG. 9. Comparisons of microscopic CDCC calculation of total reaction cross sections (solid) and neutron removal cross sections (dashed) with the experimental data [14].

The Coulomb breakup is explicitly taken into account and its contribution to the total elastic breakup cross section σ_{EB} turned out to be significant at forward angles in the case of

56 MeV incident deuteron energy on ^{208}Pb. Furthermore, its contribution to σ_{EB} was shown to be somewhat large even for light target nuclei. On the other hand, the Coulomb breakup effect on the elastic cross section was found to be negligible in all the cases investigated in the present study. The total reaction cross sections and the inclusive nucleon removal cross sections provided by ERT also agree fairly well with the experimental data, demonstrating the possible use case for other nucleon-removal cross section studies in future.

In conclusion, the microscopic CDCC, which is a microscopic effective reaction theory for deuteron-induced reactions, has been shown to be able to describe the existing experimental data for many reaction systems with no free parameters. The success of the microscopic CDCC will be of great importance for proceeding with further studies on deuteron-induced reactions in which unstable nuclei are involved.

ACKNOWLEDGMENTS

[1] M. Kamimura, M. Yahiro, Y. Iseri, Y. Sakuragi, H. Kameyama, and M. Kawai, Prog. Theor. Phys. Suppl. **89**, 1 (1986).

[2] N. Austern, Y. Iseri, M. Kamimura, M. Kawai, G. Rawitscher, and M. Yahiro, Phys. Rep. **154**, 125 (1987).

[3] M. Yahiro, K. Ogata, T. Matsumoto, and K. Minomo, Prog. Theor. Exp. Phys. (2012) 01A206.

[4] N. Austern, M. Yahiro, and M. Kawai, Phys. Rev. Lett. **63**, 2649 (1989).

[5] N. Austern, M. Kawai, and M. Yahiro, Phys. Rev. C **53**, 314 (1996).

[6] M. Yahiro, K. Minomo, K. Ogata, and M. Kawai, Prog. Theor. Phys. **120**, 767 (2008).

[7] P. Descouvemont, E. C. Pinilla, and M. S. Hussein, Few-Body Syst. **56**, 737 (2015).

[8] K. Amos, P. J. Dortmans, H. V. von Geramb, S. Karataglidis, and J. Raynnal, in *Advances in Nuclear Physics*, edited by J. W. Negele and E. Vogt (Plenum, New York, 2000), pp. 275–536.

[9] M. Toyokawa, K. Minomo, M. Kohno, and M. Yahiro, J. Phys. G: Nucl. Part. Phys. **42**, 025104 (2015).

[10] M. Toyokawa, M. Yahiro, T. Matsumoto, K. Minomo, K. Ogata, and M. Kohno, Phys. Rev. C **92**, 024618 (2015).

[11] P. Navrátil and S. Quaglioni, Phys. Rev. C **83**, 044609 (2011).

[12] R. C. Johnson and N. K. Timofeyuk, Phys. Rev. C **89**, 024605 (2014).

[13] M. Yahiro, K. Ogata, and K. Minomo, Prog. Theor. Phys. **126**, 167 (2011).

[14] N. Matsuoka, M. Kondo, A. Shimizu, T. Saito, S. Nagamachi, H. Sakaguchi, A. Goto, and F. Ohtani, Nucl. Phys. A **345**, 1 (1980).

[15] M. Toyokawa, K. Minomo, and M. Yahiro, Phys. Rev. C **88**, 054602 (2013).

[16] K. Minomo, K. Ogata, M. Kohno, Y. R. Shimizu, and M. Yahiro, J. Phys. G: Nucl. Part. Phys. **37**, 085011 (2010).

[17] R. Johnson and P. Soper, Nucl. Phys. A **182**, 619 (1972).

[18] N. K. Timofeyuk and R. C. Johnson, Phys. Rev. Lett. **110**, 112501 (2013).

[19] S. Hashimoto, M. Yahiro, K. Ogata, K. Minomo, and S. Chiba, Phys. Rev. C **83**, 054617 (2011).

[20] T. Ohmura, B. Imanishi, M. Ichimura, and M. Kawai, Prog. Theor. Phys. **43**, 347 (1970).

[21] E. Stephenson, C. Foster, P. Schwandt, and D. Goldberg, Nucl. Phys. A **359**, 316 (1981).

[22] M. Yahiro, Y. Iseri, H. Kameyama, M. Kamimura, and M. Kawai, Prog. Theor. Phys. Suppl. **89**, 32 (1986).

[23] N. Matsuoka, H. Sakai, T. Saito, K. Hosono, M. Kondo, H. Ito, K. Hatanaka, T. Ichihara, A. Okihana, K. Imai, and K. Nisimura, Nucl. Phys. A **455**, 413 (1986).

[24] F. Hinterberger, G. Mairle, U. Schmidt-Rohr, G. Wagner, and P. Turek, Nucl. Phys. A **111**, 265 (1968).

[25] G. Takeda and K. M. Watson, Phys. Rev. **97**, 1336 (1955).

[26] R. A. D. Piyadasa, M. Yahiro, M. Kamimura, and M. Kawai, Prog. Theor. Phys. **81**, 910 (1989).

[27] R. A. D. Piyadasa, M. Kawai, M. Kamimura, and M. Yahiro, Phys. Rev. C **60**, 044611 (1999).

[28] P. C. Huu-Tai, Nucl. Phys. A **773**, 56 (2006).

[29] P. C. Huu-Tai, Nucl. Phys. A **776**, 80 (2006).

[30] J. L. Yntema, Phys. Rev. **113**, 261 (1959).

[31] N. V. Sen, J. Arvieux, Y. Yanlin, G. Gaillard, B. Bonin, A. Boudard, G. Bruge, J. Lugol, R. Babinet, T. Hasegawa, F. Soga, J. Cameron, G. Neilson, and D. Sheppard, Phys. Lett. B **156**, 185 (1985).